Advancing Planar Magnetic Microswimmers: Swimming, Channel Navigation, and Surface Motion

Yasin Cagatay Duygu¹, Gokhan Kararsiz¹, Austin Liu², U Kei Cheang³, Alexander M. Leshansky⁴, and Min Jun Kim^{1,*}

Abstract-Planar magnetic microswimmers are well-suited for in vivo biomedical applications due to their cost-effective mass production through standard photolithography techniques. The precise control of their motion in diverse environments is a critical aspect of their application. This study demonstrates the control of these swimmers individually and as a swarm, exploring navigation through channels and showcasing their functional capabilities for future biomedical settings. We also introduce the capability of microswimmers for surface motion, complementing their traditional fluid-based propulsion and extending their functionality. Our research reveals that microswimmers with varying magnetization directions exhibit unique trajectory patterns, enabling complex swarm tasks. This study further delves into the behavior of these microswimmers in intricate environments, assessing their adaptability and potential for advanced applications. The findings suggest that these microswimmers could be pivotal in areas such as targeted drug delivery and precision medical procedures, marking significant progress in the biomedical and micro-robotic fields and offering new insights into their control and behavior in diverse environments.

I. INTRODUCTION

Recent research has increasingly focused on the controlled navigation of microswimmers through complex fluidic media [1], [2], [3], [4], [5]. Specifically, planar magnetic microswimmers have emerged as a promising tool for in vivo biomedical applications, recognized for their scalability and the relative simplicity of mass production through standard photolithography techniques [6], [7], [8]. These microscale robotic systems are on the cusp of transforming various fields, offering precision and versatility for targeted drug delivery [9], non-invasive surgical procedures [10], and cellular therapy [11], [12].

The study of microorganisms and bio-inspired magnetic microswimmers, especially in low Reynolds number environments, has provided a substantial foundation for advancements in this area [13], [14], [15]. Extensive theoretical and experimental analyses have been conducted on various geometries for microscale propulsion, in particular helical shape [16], [17], [18], [19], [20]. Yet, the production of these intricate structures remains complex and costly, involving

advanced techniques like biotemplated synthesis and two-photon polymerization [21], [22], [23], [24], [25], [26], [27].

In this context, planar magnetic microswimmers stand out for their simpler production process and significant potential in diverse biomedical applications [6], [7]. The achievement of precise and responsive control over their motion in fluidic environments is crucial for applications ranging from minimally invasive surgery to on-site diagnostics [28]. To achieve this aim, understanding the underlying theory of magnetically driven propulsion of an arbitrarily shaped microswimmer is essential. The theory, crucial for practical application, indicates that chirality might not be solely based on the geometry, but could also be affected by the magnetization [29], [30].

Our prior work characterized the V-shaped microswimmers' propulsion in Newtonian fluid, revealing that their experimental motion correlates well with theoretical projections, affirming the validity of our rotation-based control in practical fluid dynamics contexts [3], [31]. Building upon this preliminary work, the present study introduces enhanced capabilities of microswimmers, enabling navigation through channels and along surfaces, a substantial departure from conventional fluid-based propulsion. Such advancements not only complement existing propulsion mechanisms but also enrich the functional versatility of microswimmers. We further investigate the behavior of microswimmers with varying directions of magnetization, unveiling unique trajectory patterns that are instrumental in performing complex tasks when operating as a swarm.

In biological settings, surface motion of microrobots is essential for adaptability and functionality, particularly when fluid properties or fast flow render the standard propulsion gaits impractical. This adaptability is crucial for tasks like targeted drug delivery, navigating through the vascular system, ablation, or performing localized diagnostics and treatments, where maneuverability and precise control are critical [32], [33], [34], [35]. The ability to transition between different modes of movement and navigate across diverse environments substantially enhances the potential of microswimmers, marking a significant leap towards practical applications and versatility of these microscale robotic systems.

The successful demonstration of these enhanced functionalities boosts the potential use of planar magnetic microswimmers to a wider spectrum of biomedical and microrobotic fields, marking a significant stride towards the realization of their practical applications. This study further

^{*}Corresponding author.

¹Yasin Cagatay Duygu, Gokhan Kararsiz, and Min Jun Kim are with the Lyle School of Engineering, Southern Methodist University.

²Austin Liu is with the Harkin School.

³U Kei Cheang is with the Department of Mechanical and Energy Engineering at Southern University of Science and Technology (SUSTech).

⁴Alexander M. Leshansky is with the Department of Chemical Engineering at Israel Institute of Technology (Technion).

delves into the behavior of these microswimmers in intricate environments, assessing their adaptability and potential for advanced applications. The findings suggest that these microswimmers could be pivotal in areas such as targeted drug delivery and precision medical procedures, marking significant progress in the biomedical and microrobotics fields and offering new insights into their control and behavior in diverse environments. As we continue to experimentally investigate and understand their dynamics, we pave new paths for revolutionary approaches in medical treatment and diagnostics, setting new benchmarks in microrobotics and biomedical engineering.

II. EXPERIMENTAL SECTION

A. Fabrication of Planar Microswimmers

Conventional photolithography technology is used to fabricate planar microswimmers as described extensively in the previous work [3]. Initially, a silicon wafer is layered with a dextran sacrificial layer due to its water-soluble nature. Following this, the SU-8 2005 photoresist is applied over the dextran layer. Utilizing standard photolithography processes like soft bake, exposure, and post-exposure bake, V-shaped structures are formed. The wafer undergoes oxygen plasma treatment to remove the dextran layer, ensuring that the microswimmers and the nickel coating applied later do not release simultaneously. A magnetic quality is given to the microswimmers by depositing a thin layer of nickel (100 nm) over the SU-8 structures using electron-beam evaporation. The wafer with V-shaped microswimmers was submerged in DI water, allowing the water-soluble dextran layer to dissolve. The V-shaped microswimmers remained attached to the substrate and were not removed until the dextran layer had completely dissolved in the DI water.

B. Experimental Setup

Fig. 1 illustrates the design of the experimental setup. For observation purposes, a Nikon Eclipse-TI Microscope with a 10× lens objective lens was used. However, to encompass the whole experimental chamber in the videos with channels in the Supporting Information, a 2× objective lens was preferred. The PixelinkPL-D755CU-T camera was utilized to record experimental videos.

A MagnetobiX AG (Switzerland) MFG-100-I magnetic field generator, which can generate uniform fields without gradients and is thus well-suited for our study, was used to direct the motion of the planar microswimmers during experiments. This generator, equipped with eight electromagnetic coils, can produce both static and rotating fields, including a conically rotating magnetic field. An open-loop control approach was adopted throughout the experiments, with the magnetic field being pre-set through the generator's software interface.

C. Channel Fabrication

To prevent fluid from leaking, a polydimethylsiloxane (PDMS) chamber with a diameter of 10 mm was positioned atop a cover glass (No. 1, $22 \text{ mm} \times 30 \text{ mm}$) for experiments

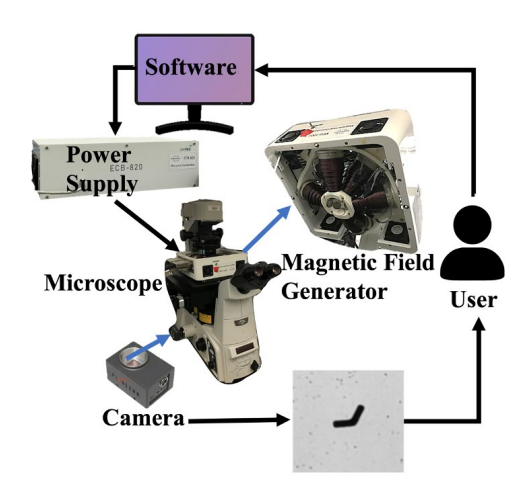


Fig. 1. For experimental purposes, the Nikon Eclipse-TI microscope is utilized. The MagnetobiX MFG-100-I creates the magnetic field, which is controlled using MBX PRO software and an ECB-820 power supply. The Pixelink PL-D755CU-T camera is used to capture the images in real time.

which PDMS channels are not used. An additional top glass was also employed to hinder evaporation, accumulation of dust, and internal fluid movement. The chamber's bottom was treated with a 20% Tween20 (Sigma-Aldrich) solution to deter the adhesion of microswimmers to the glass surface. Subsequently, a 20% NaCl solution was introduced into the chamber. The planar microswimmers were then placed inside the PDMS chamber.

Master molds were designed using SolidWorks CAD software (Dassault Systems, Velizy-Villacoublay, France), with the initial model displayed in Fig. 2(a). The detailed dimensions of the molds include flow channels measuring 1000 μ m in width and 3000 μ m in height, with inlet and outlet ports having 4000 μ m diameters, as depicted in Figs. 2(b) and 2(c). The Photron Mono 4K SLA 3D Printer was utilized to fabricate these models using Resin model R1515, achieving a layer thickness of 50 μ m, as illustrated in Fig. 2(d). Post-printing, we cleansed the molds to remove any uncured resin and then exposed them to UV light for curing over 30 minutes.

For the PDMS preparation, a 10:1 weight ratio of SYL-GARD™ 184 Silicone Elastomer Base to SYLGARD™ 184 Silicone Elastomer Curing Agent was used, with approximately 3 grams filling each mold, as shown in Fig. 2(e). The filled molds were then degassed to remove air bubbles before being cured in an oven at 85°C for 12 hours.

Upon completion of the curing, the PDMS was carefully separated from the mold to reveal the finished device, as shown in Fig. 2(f). Subsequently, plasma treatment is applied to both the PDMS channel and the glass substrate (No. 1, 22 mm x 30 mm) to ensure a strong bond between them, effectively preventing any potential leakage and ensuring a stable flow. Fluid and microswimmers are introduced into the channel through the inlet/outlet ports.

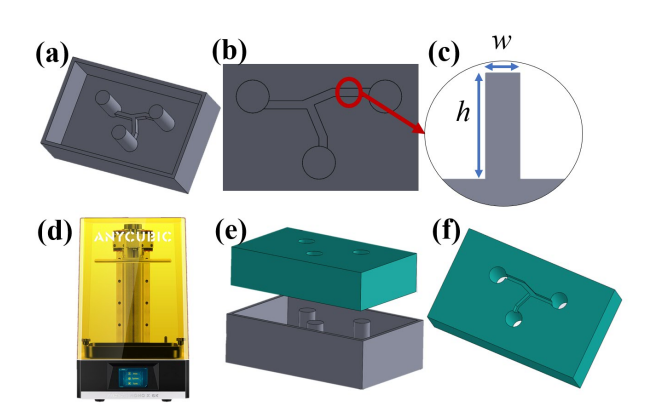


Fig. 2. a) Design of the channel structure. b) Top view of the pattern. c) Cross-sectional dimensions of the channel molds, indicating a width (w) of 1 mm and a height (h) of 3 mm. d) The SLA printer, ANYCUBIC Mono 4K, used for mold fabrication. e) Process of pouring PDMS into the mold, followed by extraction post-curing. f) The cured PDMS device displaying the embedded pattern.

III. PROBLEM FORMULATION

The microswimmers are designed with a symmetric V-shaped form, featuring a central angle of 120 degrees to optimize propulsion as suggested by prior theoretical studies, which propose that such a shape is nearly ideal for movement, and that this specific angle enhances propulsion speed [36]. The dimensions of the base are 40 μ m in length and 20 μ m in breadth, with a height of 5 μ m, giving it a height-to-width aspect ratio of 1:4. Initially, the microswimmers settle at the bottom of the chamber due to gravitational forces. During the swimming experiments, a uniform, conically rotating magnetic field, combining both a rotational and a static field along the axis of rotation, is applied as illustrated in Fig. 3(a). This figure also illustrates the swimming motion of the swimmers.

To initiate the movement of the microswimmers from the chamber's bottom, an immediate application of two orthogonal magnetic fields rotating about the X and Z axes is implemented, granting the microrobots the necessary impetus to detach from the surface if they have adhered. To circumvent boundary effects and optimize propulsion performance, this action is accompanied by a conically rotating (around the Z-axis) field, which swiftly propels the microswimmers to a height of at least 1000 μ m above the chamber floor. A subsequent application of the conically rotating magnetic field, with a static component directed along the Y-axis, is then utilized to guide the microswimmers' navigation in the YZ-plane. The gravity force, however, induces a downward motion, causing the microswimmers to sink gradually, as depicted in Fig. 3(a).

The conically rotating magnetic field **B** applied to propel microswimmers along the *Y*-axis (see Fig. 3a) is given by:

$$\mathbf{B} = \hat{\mathbf{x}}\sin(\omega t) + \hat{\mathbf{y}}\delta + \hat{\mathbf{z}}\cos(\omega t) \tag{1}$$

where δ is the ratio of the static field to rotating field components, ω is the angular frequency, and t is the time.

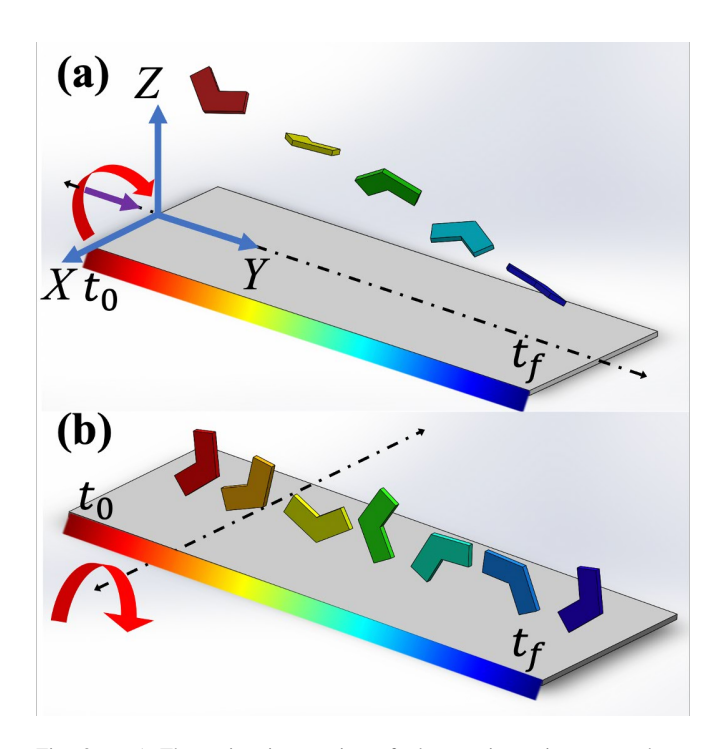


Fig. 3. a) The swimming motion of planar microswimmers under a conically rotating magnetic field is depicted with a static field indicated by the purple arrow and a rotating field by the red arrow, alongside the XYZ coordinate axes. b) This panel captures the microswimmers in a tumbling motion at the surface, with the red arrow symbolizing the rotating magnetic field. In both scenarios, the black axes represent the axes of rotation, and the microswimmers are color-coded to illustrate the progression over time from the initial (t_0) to the final (t_f) time points.

To direct the swimmers along an arbitrary three-dimensional trajectory, such as letter-shaped paths demonstrated in our experiments, we employ rotations to allow the desired three-dimensional control. These rotations are mathematically represented by the rotation matrices $R_x(\theta)$, $R_y(\theta)$, and $R_z(\theta)$, corresponding to rotations about the X, Y, and Z axes, respectively:

$$R_x(\theta) = \begin{bmatrix} 1 & 0 & 0\\ 0 & \cos(\theta) & -\sin(\theta)\\ 0 & \sin(\theta) & \cos(\theta) \end{bmatrix}, \tag{2}$$

$$R_y(\theta) = \begin{bmatrix} \cos(\theta) & 0 & \sin(\theta) \\ 0 & 1 & 0 \\ -\sin(\theta) & 0 & \cos(\theta) \end{bmatrix}, \tag{3}$$

$$R_z(\theta) = \begin{bmatrix} \cos(\theta) & -\sin(\theta) & 0\\ \sin(\theta) & \cos(\theta) & 0\\ 0 & 0 & 1 \end{bmatrix}. \tag{4}$$

The second motion gait explored in this study is surface motion. Previously, we have facilitated the vertical (or transverse, perpendicular to the bounding surface) swimming of planar microswimmers before directing them to a specific location. However, in environments where vertical motion is impeded, such as the narrow capillaries within the human body, or within rapid fluid flows similar to those occurring in arterial vessels, vertical maneuverability is restricted. These

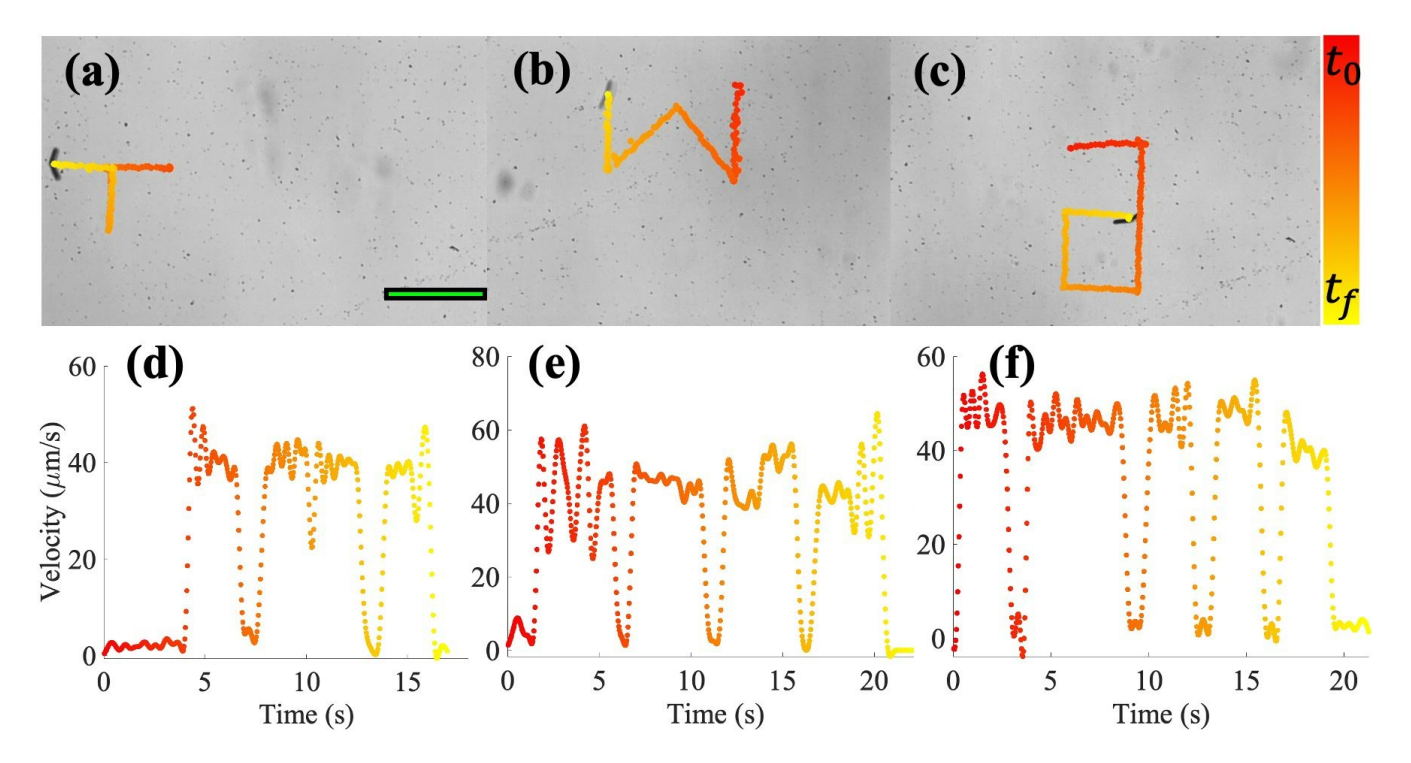


Fig. 4. a), b), and c) depict the trajectories of individual microswimmers during a swimming experiment, each shaped like the characters "T", "w", and "a", respectively. d), e), and f) correspond to the velocity profiles of the swimmers from experiments a), b), and c), over time. In the trajectory images, time is represented by a color gradient, with the scale provided in the upper right corner transitioning from initial (t_0) to final (t_f) time points. Green scale bar shows 200 μ m.

conditions require for a new way to move the microswimmers, making them more adaptable to different environments.

For example, in the tight extracellular spaces or within the intricate networks of the lymphatic system, the capacity for longitudinal motion is crucial for effective navigation. Similarly, when faced with the dynamic and often turbulent conditions present within the gastrointestinal tract, adapting to surface motion allows microswimmers to maintain stability and control.

To initiate surface motion, microswimmers are exposed to a rotational magnetic field, as demonstrated in Fig. 3(b), where the axis of rotation is perpendicular to their path of displacement. By adjusting the field's rotational axis, we finely control their direction and velocity along the bounding surface. We use rotational matrices to define these orientations in three-dimensional space, allowing for precise trajectory planning without inverse kinematics. This method opens up new possibilities for their application in complex and confined environments.

IV. EXPERIMENTAL RESULTS

A. Swimming Motion

To demonstrate the precise controllability of individual microswimmers, they were guided along predetermined trajectories shaped as the letters 'T', 'w', and 'a' using a conically rotating magnetic field as depicted in Fig.4 (a), (b), and (c). The letters stand for 'Texas, wisdom, advance', reflecting the lab's aim to push forward in microrobotics, drawing on the smart, innovative spirit of Texas.

For all swimming experiments, a rotational magnetic field with 25 mT magnitude with a frequency of 10 Hz was used with a 7.5 mT static field (δ =0.3). The average velocities of the microswimmers during each segment of the 'T' trajectory were 40.99 µm/s, 39.24 µm/s, and 38.34 µm/s, respectively. For the 'w' pattern, the corresponding average velocities were 43.81 µm/s, 45.87 µm/s, 47.4 µm/s, and 44.1 µm/s. For the 'a' formation, the average velocities recorded for the strokes were 48.48 µm/s, 46.10 µm/s, 47.53 µm/s, 48.9 µm/s and 40.52 µm/s. The velocity-time graphs for the trajectories shaped as 'T', 'w', and 'a' are presented in Fig. 4(d), (e), and (f), respectively. The results are in accord with our previous work, showing that velocity control is also possible for future applications.

The study extended to examining the behavior of swimmers magnetized in varying directions. The microswimmers are magnetized along their easy axis, all oriented in the same direction. However, fabrication imperfections occasionally resulted in a subset of swimmers being magnetized along alternate vectors, leading to distinct trajectories under the same global magnetic field. As illustrated in Fig. 5(a), two swimmers with inverse magnetization traced out a 'z' shaped path, but in opposite directions. This phenomenon suggests a novel approach to controlling swimmers as a group. By altering the direction of magnetization, it is possible to direct different swimmers along distinct routes, potentially enabling more complex collective dynamics and the execution of intricate tasks by the swarm, though this requires a high precision in the magnetization process, which can be challenging

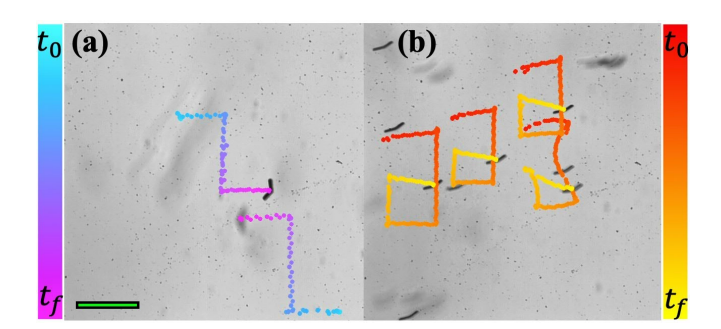


Fig. 5. a) Trajectories of individual planar microswimmers with different magnetization, indicated by a color gradient from the experiment's start (t_0) to its end (t_f) . b) Trajectory patterns of a swarm of planar microswimmers, with time progression similarly represented by a color gradient from initial (t_0) to final (t_f) time points. Green scale bar shows 200 μ m.

to scale. For instance, the use of geometric variations in microrobotic helices was demonstrated to achieve individual control, as shown in the study by Giltinan and colleagues [37]. Our previous work supports the effectiveness of swarm control irrespective of the inter-robot distances as long as the robots remain within the magnetic field generator's effective range [3]. However, if the robots get too close, they can attach due to the magnetic forces.

Experiments were also conducted to evaluate the group behavior of microswimmers, which is illustrated in Fig. 5(b), where multiple units are seen following an 'a' shaped trajectory in unison. Nonetheless, variances in trajectory paths and velocities were observed among the microswimmers. These discrepancies in velocity may stem from slight differences in the magnetization orientation and strength of individual microswimmers due to manufacturing inconsistencies. The deviations in trajectory, particularly observed in the microswimmer at the lower right-side in Fig. 5(b) drifting from the planned route, could stem from the hydrodynamic interactions between the microswimmers.

The supplementary information accompanying this paper includes a related video for Fig. 5(b) and additional videos for all other figures presented. Each spinning propeller generates a localized swirling flow, functioning effectively as a point rotlet to the leading approximation, which creates a vortex-like flow around it [38]. While this swirling does not alter the collective movement of the microswimmers, it can affect their individual paths. The influence of this flow diminishes with the square of the distance from the source, hence the behavior of nearby microswimmers is predominantly unaffected when they maintain a separation distance, l, that exceeds the size of an individual propeller[40]. Initially positioned at this separation distance l, the microswimmers experience the described hydrodynamic interactions, leading to the altered trajectories as described above.

B. Swimming through Channels

Conducting experiments within channels is crucial for biological applications, as they closely mimic the narrow, confined spaces found within living organisms, such as blood vessels, capillaries, or extracellular domains. These in vitro settings, whose fabrication is detailed in Section II.C, allow to simulate and study the behavior of microswimmers in conditions resembling realistic in vivo environments. Our objective is to demonstrate that the swimming motion can be efficiently controlled within confined channel geometry, similarly to the unpatterned chamber environment, thereby proving the potential for precise navigation in biologically relevant settings.

The propulsion direction is preprogrammed with eight cardinal and intercardinal directions (NORTH, NORTHEAST, EAST, SOUTHEAST, SOUTH, SOUTHWEST, WEST, NORTHWEST) for selection, enabling the successful steering of microswimmers in confinement, as shown in Fig. 6(a), (b), and (c). It is, however, crucial to note the environmental factors that may alter a microswimmer's path, as illustrated in Fig. 6(a). When directed WEST and then NORTH, the swimmer on the upper-right side inadvertently moves EAST due to an instantaneous flow in that region, while the swimmer on the lower-left remains unaffected and propels directly northward. Additionally, in the latter part of the experiment, the swimmer on the upper-right propels at a greater speed than its lower-left counterpart. This variation in speed could be attributed to transient flows, possibly arising from a leak between the glass and PDMS device or from other factors, given that the channel is open on its top side. The average velocity of the microswimmers throughout the experiment varied due to these environmental factors.

In Fig. 6(b), the user navigates the robots SOUTH then EAST, with the expectation that the swimmers will follow the channel's bifurcation outline. Particularly, the inputs were based on the position of the microswimmer at the bottom, leading to the upper swimmer colliding with the channel wall when moving EAST. This outcome underscores the necessity of comprehensive path-planning for all microswimmers to prevent collisions. Future work will focus on implementing path-planning and closed-loop control systems to enable the efficient and simultaneous steering of multiple swimmers. The velocities of the two swimmers varied, with the specifics detailed in the corresponding section of the results. Fig. 6(c) presents a scenario where both swimmers are accounted for in the experiment, leading to their successful navigation along the channel configurations. The average velocities observed in this part did not show a significant change

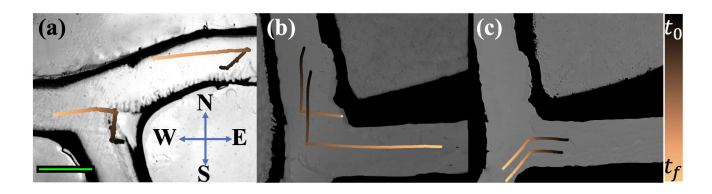


Fig. 6. (a) Microswimmers' path through channels, depicted with a color gradient indicating the progression from start to finish of the swim. (b) and (c) Show microswimmers in identical channels, with their swimming trajectories marked by a color gradient representing the duration of the experiment from initial (t_0) to final (t_f) time points. Green scale bar shows 1mm. N,W,S, and E shows the NORTH, WEST, EAST, and SOUTH directions

compared to the experiments illustrated in Fig. 4(a), 4(b), and 4(c), with average velocities ranging between 39.2 μ m/s and 46.6 μ m/s.

C. Surface Motion

The second motion mode explored in this study is surface motion. Previously, we have facilitated the transverse swimming of planar microswimmers before directing them to a specific location. However, in environments where transverse motion is impeded, such as the narrow capillaries within the human body, or channels with rapid flows such that found in large arterial vessels, transverse maneuverability is restricted. These conditions necessitate an alternative motion gait to enhance the maneuverability of the microswimmers. For example, in the tight spaces within extracellular domains or the intricate networks of the lymphatic system, the capacity for surface motion is crucial for effective navigation. Similarly, when faced with the dynamic and often turbulent conditions present within the gastrointestinal tract, adapting to surface motion allows microswimmers to maintain stability and control.

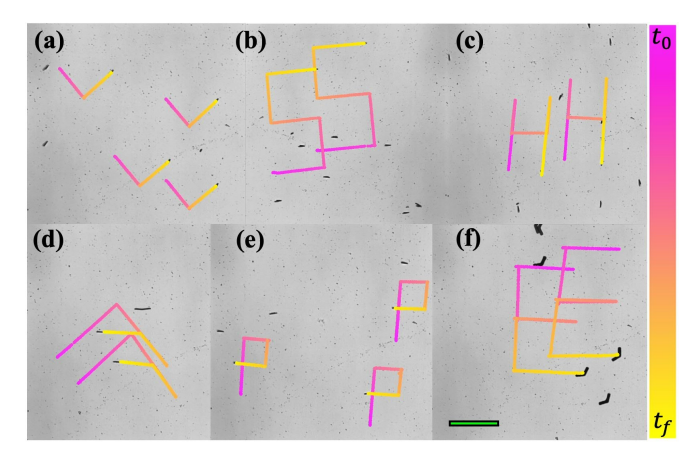


Fig. 7. . (a) Microswimmers' path through channels, depicted with a color gradient indicating the progression from start to finish of the swim. (b) and (c) Show microswimmers in identical channels, with their swimming trajectories marked by a color gradient representing the duration of the experiment from initial (t_0) to final (t_f) time points. Green scale bar shows 1mm. N,W,S, and E shows the NORTH, WEST, EAST, and SOUTH directions.

To initiate surface motion, the microswimmers are exposed to an in-plane rotational magnetic field. This is demonstrated in Fig. 3(b), where the axis of rotation is perpendicular to the microswimmers' path of displacement. By adjusting the field's rotational axis, we can precisely control the direction and velocity of the microswimmers along the surface, opening the new possibilities for their application in complex and dynamic environments.

Fig. 7(a)-(f) illustrate the controlled surface movement of the planar microswimmers, precisely following the outlined paths for the letters V-SHAPE. The average velocity recorded was 11.72 μ m/s, which is considerably lower than the velocity achieved in swimming mode. The experiments were conducted with a 5 mT in-plane rotating magnetic field at a frequency of 1 Hz. A key observation is that when

the frequency exceeds 1.5 Hz, the microswimmers begin to deviate from their anticipated path during rolling, which results in a loss of control over the motion. Investigating this frequency-velocity relationship could be an intriguing avenue for future research, potentially leading to improved control strategies for microswimmers in various operational modes.

V. CONCLUSIONS

This research represents a substantial step forward in the utilization of planar magnetic microswimmers, showcasing their refined navigation through complex environments and their potential for biomedical applications. The incorporation of surface (rolling) motion alongside navigation in channels, significantly expands their operational versatility. Possessing the capability to adapt to different magnetization directions, these microswimmers offer flexible control which holds promise for applications in medical treatments, including targeted drug delivery and accurate diagnostic procedures.

The enhanced control and adaptability of microswimmers for navigating the human body's narrow spaces advance their practical use and open avenues for complex swarm operations in medical technology. While in vivo application poses challenges in tracking and feedback, future research aims to overcome these through advanced non-visual pose estimation techniques, setting the stage for innovative microrobotic healthcare solutions.

APPENDIX

Supplementary videos that demonstrate the dynamics depicted in Fig. 4, 5, 6, and 7 are available. These videos extend the static images in the paper, illustrating the microswimmers' movement and interaction with each other in real-time.

ACKNOWLEDGMENT

This work was financially supported by the United States–Israel Binational Science Foundation (#2021657), the National Science Foundation (CMMI #2123824), the Guangdong Basic and Applied Basic Research Foundation(2023A1515012229), the Department of Education of Guangdong(2021ZDZX2037), and the Science and Technology Innovation Committee Foundation of Shenzhen (RCYX20210609103644015). The authors acknowledge the technical support provided by the SUSTech Core Research Facilities (SCRF) for the fabrication of V-shaped microswimmers.

REFERENCES

- G. Dogangil, O. Ergeneman, J. J. Abbott, S. Pané, H. Hall, S. Muntwyler, and B. J. Nelson, "Toward targeted retinal drug delivery with wireless magnetic microrobots," in 2008 IEEE/RSJ International Conference on Intelligent Robots and Systems. IEEE, 2008, pp. 1921– 1926
- [2] M. Li, X. Hu, Y. Zhao, and N. Jiao, "An overview of recent progress in micro/nanorobots for biomedical applications," *Advanced Materials Technologies*, vol. 8, no. 11, p. 2201928, 2023.
- [3] Y. C. Duygu, U. K. Cheang, A. M. Leshansky, and M. J. Kim, "Propulsion of planar v-shaped microswimmers in a conically rotating magnetic field," *Advanced Intelligent Systems*, vol. 6, no. 1, p. 2300496, 2024.

- [4] D. Zhang, T. E. Gorochowski, L. Marucci, H.-T. Lee, B. Gil, B. Li, S. Hauert, and E. Yeatman, "Advanced medical micro-robotics for early diagnosis and therapeutic interventions," *Frontiers in Robotics* and AI, vol. 9, p. 1086043, 2023.
- [5] P. Liao, L. Xing, S. Zhang, and D. Sun, "Magnetically driven undulatory microswimmers integrating multiple rigid segments," *Small*, vol. 15, no. 36, p. 1901197, 2019.
- [6] J. Xiong, J. Zhang, Y. Zhong, X. Song, H. Wang, and U. K. Cheang, "Magnetically-actuated hydrogel-based achiral planar microswimmers for sers detection: In situ coprecipitation for continuous loading of iron oxide nanoparticles," *Frontiers in Bioengineering and Biotechnology*, vol. 11, p. 1086106, 2023.
- [7] Z. Chen, Z. Wang, D. Quashie Jr, P. Benhal, J. Ali, M. J. Kim, and U. K. Cheang, "Propulsion of magnetically actuated achiral planar microswimmers in newtonian and non-newtonian fluids," *Scientific Reports*, vol. 11, no. 1, p. 21190, 2021.
- [8] S. Tottori and B. J. Nelson, "Controlled propulsion of two-dimensional microswimmers in a precessing magnetic field," *Small*, vol. 14, no. 24, p. 1800722, 2018.
- [9] V. Sridhar, E. Yildiz, A. Rodríguez-Camargo, X. Lyu, L. Yao, P. Wrede, A. Aghakhani, B. M. Akolpoglu, F. Podjaski, B. V. Lotsch, et al., "Designing covalent organic framework-based light-driven microswimmers toward therapeutic applications," Advanced Materials, vol. 35, no. 25, p. 2301126, 2023.
- [10] G. Kararsiz, Y. C. Duygu, L. W. Rogowski, A. Bhattacharjee, and M. J. Kim, "Rolling motion of a soft microsnowman under rotating magnetic field," *Micromachines*, vol. 13, no. 7, p. 1005, 2022.
- [11] W. Jing and D. Cappelleri, "A magnetic microrobot with in situ force sensing capabilities," *Robotics*, vol. 3, no. 2, pp. 106–119, 2014.
- [12] K. Bente, A. Codutti, F. Bachmann, and D. Faivre, "Biohybrid and bioinspired magnetic microswimmers," *Small*, vol. 14, no. 29, p. 1704374, 2018.
- [13] E. M. Purcell, "Life at low reynolds number," in *Physics and our world: reissue of the proceedings of a symposium in honor of Victor F Weisskopf.* World Scientific, 2014, pp. 47–67.
- [14] U. K. Cheang, D. Roy, J. H. Lee, and M. J. Kim, "Fabrication and magnetic control of bacteria-inspired robotic microswimmers," *Applied Physics Letters*, vol. 97, no. 21, 2010.
- [15] J. Ali, U. K. Cheang, J. D. Martindale, M. Jabbarzadeh, H. C. Fu, and M. Jun Kim, "Bacteria-inspired nanorobots with flagellar polymorphic transformations and bundling," *Scientific reports*, vol. 7, no. 1, p. 14098, 2017.
- [16] O. Felfoul, M. Mohammadi, S. Taherkhani, D. De Lanauze, Y. Zhong Xu, D. Loghin, S. Essa, S. Jancik, D. Houle, M. Lafleur, et al., "Magneto-aerotactic bacteria deliver drug-containing nanoliposomes to tumour hypoxic regions," *Nature nanotechnology*, vol. 11, no. 11, pp. 941–947, 2016.
- [17] X. Yan, Q. Zhou, M. Vincent, Y. Deng, J. Yu, J. Xu, T. Xu, T. Tang, L. Bian, Y.-X. J. Wang, et al., "Multifunctional biohybrid magnetite microrobots for imaging-guided therapy," *Science robotics*, vol. 2, no. 12, p. eaaq1155, 2017.
- [18] B. E.-F. de Ávila, P. Angsantikul, J. Li, M. Angel Lopez-Ramirez, D. E. Ramírez-Herrera, S. Thamphiwatana, C. Chen, J. Delezuk, R. Samakapiruk, V. Ramez, et al., "Micromotor-enabled active drug delivery for in vivo treatment of stomach infection," Nature communications, vol. 8, no. 1, p. 272, 2017.
- [19] U. Kei Cheang, K. Lee, A. A. Julius, and M. J. Kim, "Multiple-robot drug delivery strategy through coordinated teams of microswimmers," *Applied physics letters*, vol. 105, no. 8, 2014.

- [20] B. J. Nelson and K. E. Peyer, "Micro-and nanorobots swimming in heterogeneous liquids," Acs Nano, vol. 8, no. 9, pp. 8718–8724, 2014.
- [21] M. A. Zeeshan, R. Grisch, E. Pellicer, K. M. Sivaraman, K. E. Peyer, J. Sort, B. Özkale, M. S. Sakar, B. J. Nelson, and S. Pané, "Hybrid helical magnetic microrobots obtained by 3d template-assisted electrodeposition," *Small*, vol. 10, no. 7, pp. 1284–1288, 2014.
- [22] L. Zhang, J. J. Abbott, L. Dong, B. E. Kratochvil, D. Bell, and B. J. Nelson, "Artificial bacterial flagella: Fabrication and magnetic control," *Applied Physics Letters*, vol. 94, no. 6, 2009.
- [23] X. Yan, Q. Zhou, J. Yu, T. Xu, Y. Deng, T. Tang, Q. Feng, L. Bian, Y. Zhang, A. Ferreira, et al., "Magnetite nanostructured porous hollow helical microswimmers for targeted delivery," Advanced Functional Materials, vol. 25, no. 33, pp. 5333–5342, 2015.
- [24] D. Walker, M. Kubler, K. Morozov, P. Fischer, and A. Leshansky, "Optimal length of low reynolds number nanopropellers," *Nano letters*, vol. 15, no. 7, pp. 4412–4416, 2015.
- [25] E. J. Smith, D. Makarov, S. Sanchez, V. M. Fomin, and O. G. Schmidt, "Magnetic microhelix coil structures," *Physical review letters*, vol. 107, no. 9, p. 097204, 2011.
- [26] W. Gao, X. Feng, A. Pei, C. R. Kane, R. Tam, C. Hennessy, and J. Wang, "Bioinspired helical microswimmers based on vascular plants," *Nano letters*, vol. 14, no. 1, pp. 305–310, 2014.
- [27] C. Peters, O. Ergeneman, P. D. W. García, M. Müller, S. Pané, B. J. Nelson, and C. Hierold, "Superparamagnetic twist-type actuators with shape-independent magnetic properties and surface functionalization for advanced biomedical applications," *Advanced Functional Materials*, vol. 24, no. 33, pp. 5269–5276, 2014.
- [28] E. Gutman and Y. Or, "Simple model of a planar undulating magnetic microswimmer," *Physical Review E*, vol. 90, no. 1, p. 013012, 2014.
- [29] K. I. Morozov, Y. Mirzae, O. Kenneth, and A. M. Leshansky, "Dynamics of arbitrary shaped propellers driven by a rotating magnetic field," *Physical Review Fluids*, vol. 2, no. 4, p. 044202, 2017.
- [30] J. Sachs, K. I. Morozov, O. Kenneth, T. Qiu, N. Segreto, P. Fischer, and A. M. Leshansky, "Role of symmetry in driven propulsion at low reynolds number," *Physical Review E*, vol. 98, no. 6, p. 063105, 2018.
- [31] K.-J. Cohen, B. Y. Rubinstein, O. Kenneth, and A. M. Leshansky, "Unidirectional propulsion of planar magnetic nanomachines," *Physical Review Applied*, vol. 12, no. 1, p. 014025, 2019.
- [32] B. J. Nelson, I. K. Kaliakatsos, and J. J. Abbott, "Microrobots for minimally invasive medicine," *Annual review of biomedical engineering*, vol. 12, pp. 55–85, 2010.
- [33] H. Zeng, Y. Wang, T. Jiang, H. Xia, X. Gu, and H. Chen, "Recent progress of biomimetic motions—from microscopic micro/nanomotors to macroscopic actuators and soft robotics," *RSC advances*, vol. 11, no. 44, pp. 27406–27419, 2021.
- [34] J. Wang and W. Gao, "Nano/microscale motors: biomedical opportunities and challenges," ACS nano, vol. 6, no. 7, pp. 5745–5751, 2012.
- [35] G. Kararsiz, Y. C. Duygu, Z. Wang, L. W. Rogowski, S. J. Park, and M. J. Kim, "Navigation and control of motion modes with soft microrobots at low reynolds numbers," *Micromachines*, vol. 14, no. 6, p. 1209, 2023.
- [36] Y. Mirzae, O. Dubrovski, O. Kenneth, K. I. Morozov, and A. M. Leshansky, "Geometric constraints and optimization in externally driven propulsion," *Science robotics*, vol. 3, no. 17, p. eaas8713, 2018.
- [37] J. Giltinan, P. Katsamba, W. Wang, E. Lauga, and M. Sitti, "Selectively controlled magnetic microrobots with opposing helices," *Applied Physics Letters*, vol. 116, no. 13, 2020.
- [38] S. Kim and S. J. Karrila, Microhydrodynamics: principles and selected applications. Butterworth-Heinemann, 2013.